論文 / 著書情報
Article / Book Information

Title	DYNAMIC CHARACTERISTICS OF SEISMICALLY ISOLATED HIGH-RISE BUILDING BASED ON SEISMIC RESPONSE RECORDS
Authors	J. Wu, D. Sato
Pub. date	2020, 9
Citation	2020 17WCEE Proceedings

DYNAMIC CHARACTERISTICS OF SEISMICALLY ISOLATED HIGH-RISE BUILDING BASED ON SEISMIC RESPONSE RECORDS

J. Wu[1] and D. Sato[2]

[1] *Graduate Student, School of Environment and Society, Tokyo Institute of Technology, go.k.aa@m.titech.ac.jp*
[2] *Associate Prof., FIRST, Tokyo Institute of Technology, sato.d.aa@m.titech.ac.jp*

Abstract

Seismic isolation technology for buildings began to attract attention in Japan since the 1995 Great Hanshin-Awaji Earthquake. In recent years, the number of cases where seismic isolation has been adopted for high-rise buildings has increased, and this demand is expected to continuously grow. Seismically isolated high-rise buildings tend to have long natural periods, and are therefore susceptible to wind. As such, wind loads are becoming important external design forces along with seismic loads. There are many unclear points about the consistency of the numerically modeled building and the actual building wind responses that are needed to be grasped. Analytical investigation is vital in grasping the wind response characteristics. As of the conduct of this study, there are few reports in Japan that analyzed seismically isolated high-rise building based on observation records. Reasons for this are: (1) observed wind responses have longer duration and a smaller amplitude than the earthquake response, and (2) unlike earthquakes, it is impossible to observe the wind force acting on buildings.

Addressing above, this paper builds a model of seismically isolated high-rise building (20-floor building) for wind response analysis. The dynamic characteristics are identified based on multiple seismic observation records of different levels, such as those with the same amplitude as the wind response observation records and those with large amplitudes of large earthquake levels. From the seismic response observation records, the layer structure and stiffness of the base isolation layer are identified. The curve fitting method of the transfer function is applied to the superstructure that identifies the attenuation by dividing it into the superstructure and the seismic isolation layer. The input wave is applied at the center of gravity of the 2nd floor directly above the seismic isolation layer, and the output wave is taken at the 20th floor. Seismic isolation layer is considered to have energy absorption such as frictional elements or viscous elements. The total absorbed energy is determined by trial-and-error so that the absorbed energy at the end of the vibration is less than 1%. The equivalent attenuation constant is then calculated from the largest loop of the history curve. As described above, the earthquake response analysis is performed using the identified model, and the analysis results are compared with the maximum observed wind response and the time history waveform.

Fig. 1 shows an example of the maximum observed and predicted accelerations ($Acc._{max}$) along the building height. It can be confirmed that the predicted response of the model and the observed response agree well in both X- and Y-directions. Therefore, the model which identifies the dynamic characteristics of the seismically isolated high-rise building based on the seismic response observation record, and that the response is reproduced accurately.

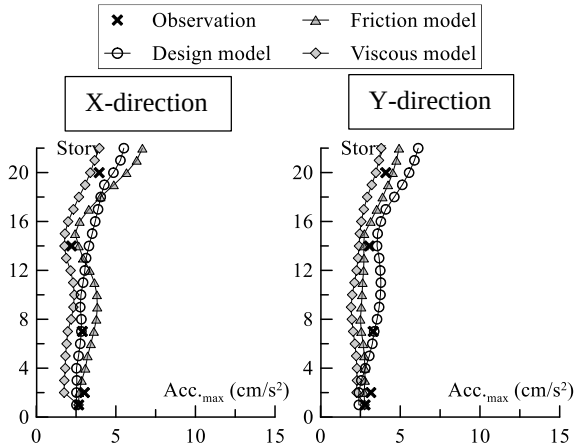

Figure 1 Maximum acceleration

Keywords: seismically isolated high-rise building; multiple seismic observation records; response history analysis

1. Introduction

In Japan, seismically isolated buildings began to attract attention following the 1995 Great Hanshin-Awaji Earthquake. The reliability of seismically isolated buildings was reconfirmed in the Great East Japan Earthquake that occurred in 2011, and in recent years the use of seismically isolated structures in high-rise buildings has been increasing, and demand is expected to continue to increase in the future. Since the high-rise base-isolated building tends to have a longer natural period than a normal base-isolated building, is easily affected by the wind, and the seismic isolated layer may be plasticized, the wind load is important together with the seismic load. It is an external force for design. Therefore, an analysis by analysis at the design stage is indispensable to grasp the wind response characteristics. However, at present the data on the design of seismically isolated buildings is not sufficient.

To date, there have been many studies analyzing the dynamic characteristics of seismically isolated buildings based on seismic response observation records with large amplitudes[1-2]. However, few cases have analyzed the dynamic behavior of base-isolated buildings based on wind response observation records [3]. The reason is that in order to correctly evaluate the wind response, it is desirable to consider the wind response time history analysis at the design stage. However, since the amplitude of the response differs greatly between the seismic response and the wind response, the rigidity and damping of the analysis model are considered. It is considered that the structural characteristics of the building differ, and there are many unclear points about the consistency between the analysis model and the dynamic characteristics of the actual building. In addition, since wind power cannot be measured directly, there are few examples of evaluation based on wind response observation records. Among them, only the research by Wu *et al.* [3] is a report on actual behavior under strong wind based on actual measurements of a high-rise base-isolated building where the effect of wind load is large. In order to accurately evaluate the wind response of a high-rise base-isolated building, the authors reported a study on grasping the dynamic characteristics of the building from seismic observation records of the high-rise base-isolated building and constructing a model for wind response analysis. [3]. Here, the identification model constructed from one seismic observation record is smaller than the design model based on the design documents with respect to the observed value, but is still about 2-3 times larger than the response of the observed value. It was confirmed that there was a gap. However, it has been shown that the identification results may have amplitude dependence [3]. Therefore, the evaluation in Ref. 3) may be insufficient.

Therefore, in this paper, to build a model for wind response analysis, the upper seismic isolation based on multiple seismic observation records, such as those with the same amplitude as the wind response observation records and those with large earthquake level amplitudes, was used. Identify the dynamic characteristics of buildings and analyze them from multiple angles. In addition, evaluation is performed by comparing with the observed values of each element assigned to the seismic isolation layer.

2. Organization

2.1 Overview of target building and observation system

The building targeted in this paper is the J2 building located on the Tokyo Institute of Technology campus. Fig. 1 shows an elevation view of the J2 building. The J2 building has a direct foundation, 20 floors above ground, and 2 floors of towers. The superstructure is 83 m high, with a boarding ratio (H/√BD) of 3.1 and a side length ratio (B / D) of 3 It is a super high-rise seismic isolation building with a flat shape. The design natural period is 4.2 s in the X direction and 4.4 s in the Y direction. Fig. 2 shows the layout of the

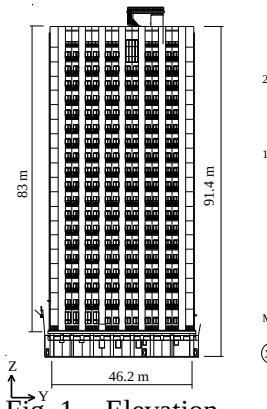

Fig. 1 – Elevation view of J2 building

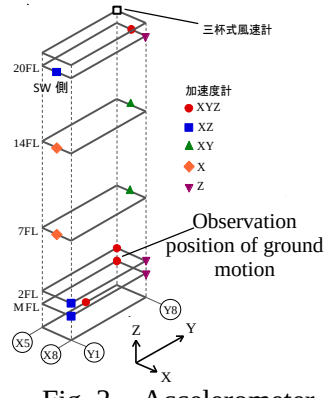

Fig. 3 – Accelerometer installation position

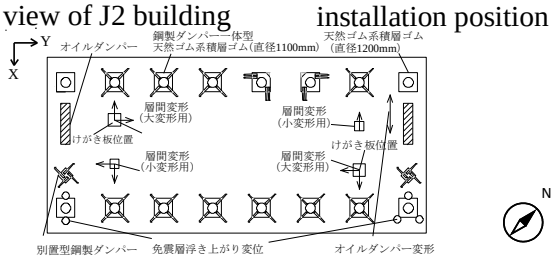

Fig. 2 – Disposition of base isolation layer displacement meter and seismic isolation device

seismic isolation device. The seismic isolation layer consists of a total of 16 1100mm diameter steel integrated dampers, 1200mm natural rubber laminated rubber (NRB1100, NRB1200), 2 separate steel dampers, and 2 oil dampers (X direction only). You. Steel dampers yield at 3.17 cm. Fig. 2 shows the location of the seismic isolation layer displacement meter. Fig. 3 shows the location of the accelerometer. Displacement meters are installed on the seismic isolation layer, and accelerometers are installed on the edge of the building on the 2, 7, 14, and 20-story floor, and are constantly monitored. Although the torsional component is included in the data of the displacement meter and the accelerometer in the X direction, the torsional component can be removed from the average of the output of each layer since the position of the center of gravity is located at the center in a plane [3]. Observed every 0.01 seconds in time steps. Since the displacement and accelerometer records have been continuously observed for a long time, the zero point shifts. In the case of an earthquake response, the average value of 500 data from the start of measurement is subtracted from the entire event of displacement and acceleration recording, and zero point correction is performed. In the case of wind response, if the top wind speed UH is 5m / s or less, it is judged as a breeze where the seismic isolation layer is not displaced, and zero point correction is performed [3]. In addition, 3 Hz or more in displacement recording and 0.1 Hz or less and 30 Hz or more in acceleration recording were judged as noise, and a low-pass or band-pass filter was applied.

Fig. 3 shows the installation position of the wind direction and wind speed measurement device. Wind direction and wind speed are constantly observed on the north side of the building top. The wind speed is recorded as the average wind speed every 3 seconds, and this is the instantaneous wind speed [3]. The average wind speed is the average value for 10 minutes. The wind direction is recorded in 16 normal directions.

2.2 Summary of wind and wind response observation records

In this paper, we analyze using Typhoon No. 20 (T0720) on October 27, 2007. T0720 is the data of the strong wind event with the highest maximum instantaneous wind speed among the observation data at the time of the J2 building alone. Fig. 4 shows the wind direction and wind speed of the entire strong wind event. T0720 passed the south side of J2 building and recorded the maximum instantaneous wind speed at the top of J2 building at 16:20. The maximum average wind speed of this typhoon was about one year during the recall period. Table 1 shows the outline of the wind observation record, and Fig. 5 shows the time history waveform of the seismic isolation layer displacement δ_0 for 10 minutes (16:20 to 16:30) when the maximum instantaneous wind speed occurs. The wind direction is the NNW direction, which is almost directly facing the long side.

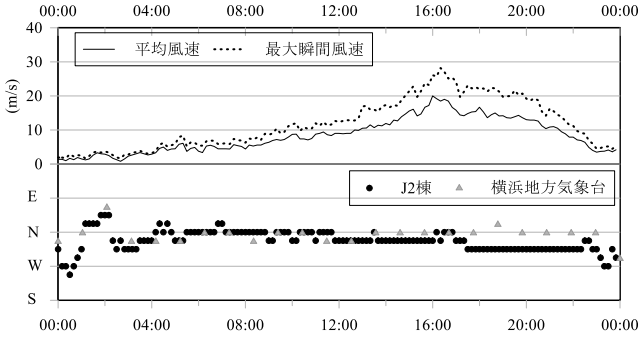

Fig. 4 Wind speed and direction

Table 1 outline of wind response observation record

年月日	平均風速 (m/s)		最大瞬間風速(m/s)		免震層 平均変位 (cm)		免震層 最大変位 (cm)	
	風速	風向	風速	風向	X	Y	X	Y
07/10/27	18.5	NNW	28.2	NNW	0.303	0.113	0.676	0.257

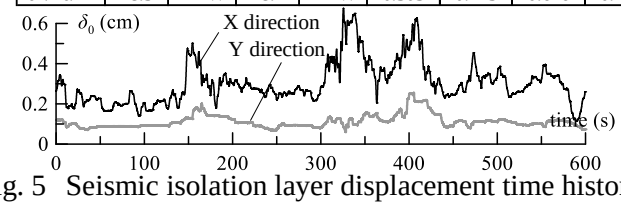

Fig. 5 Seismic isolation layer displacement time history waveform at maximum instantaneous wind speed generation time of 10 minutes（16:20，NNW direction）

2.3 Outline of earthquake and seismic response observation records

First, the maximum value of the fluctuation component of the seismic isolation layer in the X direction at T0720 is defined as δ_{0max}', and the maximum displacement of the seismic isolation layer in the X direction in the seismic response observation record is defined as δ_{0max}. In this paper, we examine seismic response observation records obtained from July 23, 2005 to September 27, 2011 at the J2 building. Among them, the characteristics of the building are identified and analyzed using the data of the seismic isolation layer X direction of 0.1 cm or more. Table 2 shows the outline of the seismic observation record. Here, from the seismic

response observation records of the J2 building, the Tokaidonanhou-Oki earthquake (TK) whose δ0max value was closest to δ_{0max}' was selected. In addition, the three waves of the Fukushima-Oki Earthquake (FK), whose δ_{0max} is about half the value of TK, and the Surugawan-Oki Earthquake (SG), which is about three times the value of TK, are mainly used. I will show you. Fig. 6 shows the acceleration time history response waveform of the observation record.

In this paper, in order to construct an equivalent shear model of 22 mass points using the above-mentioned seismic response observation records, in Chapter 3, we identify the upper structure and Chapter 4 identify the vibration characteristics of the base-isolated layer.

3. Superstructure identification based on seismic response observation records

3.1 Identification of vibration characteristics of superstructure

In this section, the transfer function curve fitting method is applied to identify the damping constant of the superstructure from the seismic observation records of the J2 building [3]. Here, the damping characteristics of the superstructure are confirmed by setting the input to the center of gravity of the second floor directly above the seismic isolation layer and the output to the 20th floor. Fig. 8 shows the results of curve fitting of the transfer function | H | smoothed with a bandwidth of 0.02 Hz. Fig. 9 shows the results of curve fitting of the phase | θ | smoothed with a bandwidth of 0.02 Hz. Note that fitting was performed in the range of 0.1 Hz to 5 Hz in order to accurately estimate up to the secondary mode in each axial direction. From Fig. 8 and Fig. 9, it can be seen that the amplitude of the transfer function agrees well with the theoretical curve.

Table 3 shows the calculated primary and secondary frequencies f_1, f_2 and damping constants h_1, h_2 of the three observation records. From Table 3, the damping constant calculated here is higher than the value h=1%[3] assumed at the time of design. Fig. 10 shows the relationship between the identified natural frequency and damping constant for the maximum acceleration A_{20max} of the 20th layer. From Fig. 10, it is clear that the natural frequency in the X and Y directions has little variation in this response range, and there is no amplitude dependence. Although the damping constant varies, no specific tendency depending on the amplitude is observed.

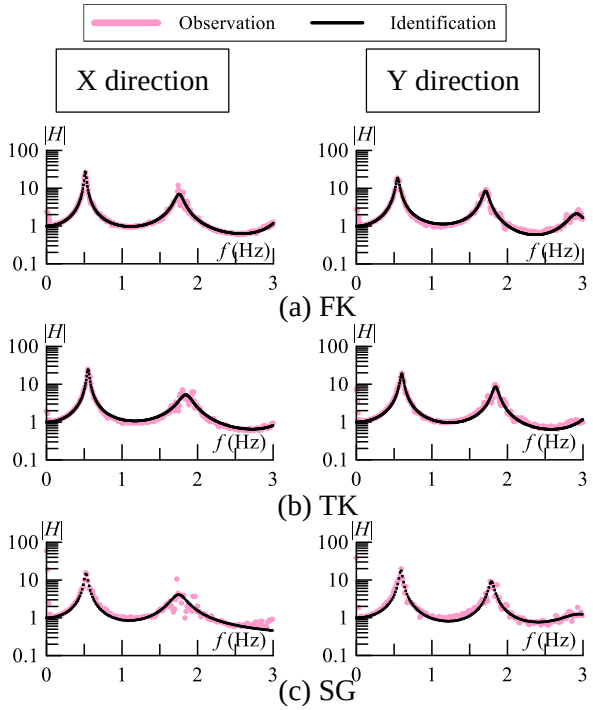

Fig. 8 Curve fitting of transfer function

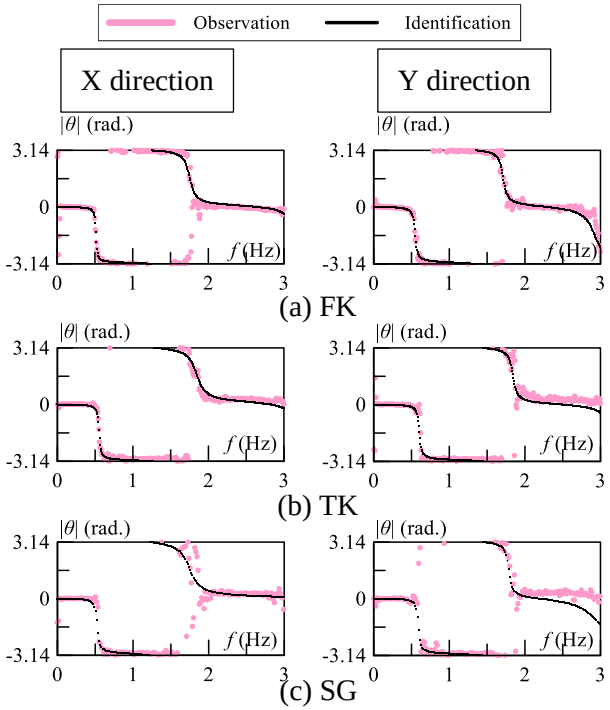

Fig. 9 Curve fitting of transfer function

Table 3 Damping ration and

(a) FK

	Frequency (Hz)		Damping ration (%)	
	1st	2nd	1st	2nd
X direction	0.51	1.75	2.44	3.10
Y direction	0.55	1.71	3.84	2.31

(b) TK

	Frequency (Hz)		Damping ration (%)	
	1st	2nd	1st	2nd
X direction	0.55	1.85	2.82	4.56
Y direction	0.60	1.84	3.41	2.18

(c) SG

	Frequency (Hz)		Damping ration (%)	
	1st	2nd	1st	2nd
X direction	0.53	1.75	4.00	5.58
Y direction	0.59	1.79	3.31	1.78

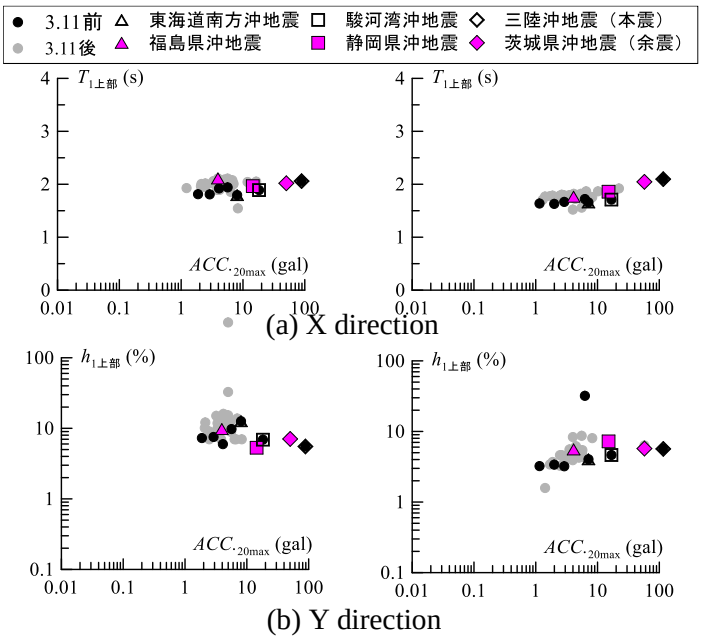

(a) X direction

(b) Y direction

Fig. 10 Relationship between identification result and maximum acceleration

3.2 Analysis of layer stiffness of superstructure

In this section, the layer stiffness of each layer is determined in the same way as in Ref. 3) and compared with the design values. However, in Ref. 3), the layer stiffness was evaluated on the assumption that the superstructure is stiffness proportional damping, but modeling is performed using Rayleigh damping. The outline of the method is described below.

The interlayer displacement $\delta_i(t)$ is calculated by integrating the difference between the absolute accelerations of the upper and lower floors by the second order (Eq. (1)). In the layer where the accelerometer is not installed, it was calculated by linearly interpolating the records of the upper and lower accelerometers. However, since the acceleration of layers 21 and 22 cannot be estimated by linear interpolation, it is assumed that the response is the same as that of layer 20, and the mass of layers 21 and 22 is incorporated into the mass of layer 20 [3].

$$\delta_i(t) = \iint \left(\ddot{X}_{i+1}(t) - \ddot{X}(t) \right) dt \tag{1}$$

Here, i = 1, 2,..., N.

The shear force of each layer considering Rayleigh damping is calculated by Eq. (2).

$$Q_i(t) = \alpha_M \left(\sum_{j=i}^{N} m_j \dot{x}_j(t) \right) + \alpha_K k_i \dot{\delta}_i(t) + k_i \delta_i(t) \tag{2}$$

Where $Q_i(t)$ is the shear force of the i-layer, mi is the mass of the i-layer, k_i is the layer stiffness of the i-layer, δ_i is the interlayer displacement of the i-layer, is the relative velocity, and α_M and α_K are the coefficients of Rayleigh damping. is there. The mass shall be set based on the design documents.

As can be seen from Eq. (2), $Q_i(t)$ includes the relative velocity up to the i-th layer, so that the layer stiffness cannot be directly evaluated from the hysteresis curve with the interlayer displacement δ_i as in Ref. Therefore, the Eq. (2) is converted to the Eq. (3), and the layer shear force $Q_i'(t)$ including only the interlayer displacement δ_i is calculated.

$$Q_i'(t) = Q_i(t) - \alpha_M \left(\sum_{j=i}^{N} m_j \dot{x}_j(t) \right) = \alpha_K k_i \dot{\delta}_i(t) + k_i \delta_i(t) \tag{3}$$

The hysteresis curve of δ_i–Q_i' is approximated by a straight line passing through the origin by the least squares method, and the layer rigidity K_i is calculated as a gradient thereof. Fig. 11 shows an example of the comparison between the calculated layer stiffness K and the design value. Note that the layer stiffness obtained from Fig. 11 showed variations that could be attributed to the effects of noise and the like included in the observation records, and in particular, the identification values above the 15 layers showed large variations. Constructing a structural model using this will cause inconsistencies with the natural frequency identified in the previous section. Therefore, in this paper, the ratio β_{Ki} between the identification value and the design value of each layer was averaged for 3 to 14 layers, and the ratio was multiplied by the design value to construct an identification model of the superstructure. Table 4 shows the magnification β_K uniformly applied to the design rigidity of the superstructure in the three observation records. Fig. 12 shows the height distribution of the rigidity of the superstructure of the identification model in comparison with the design value.

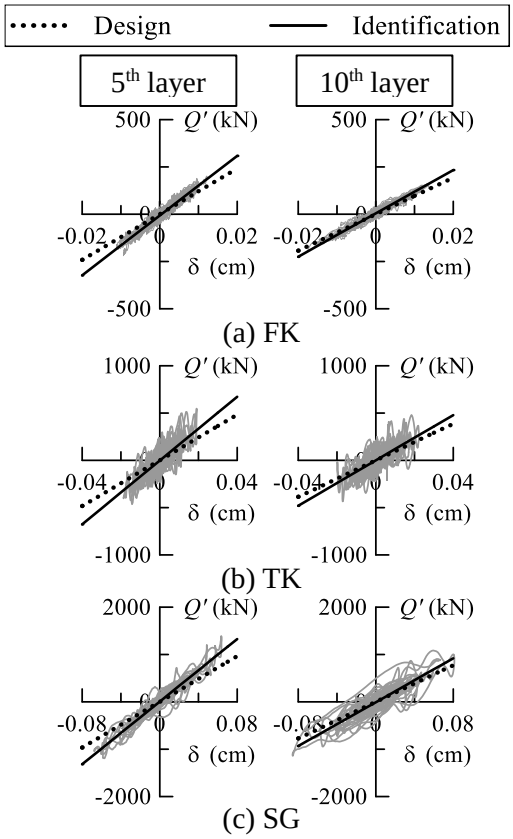

Fig. 11 Histeresis loop of seismic isolation layer

Table 4 Magnification for design stiffness

	FK		TK		SG	
	X	Y	X	Y	X	Y
β_{Ki}	1.23	1.73	1.30	1.70	1.25	1.56

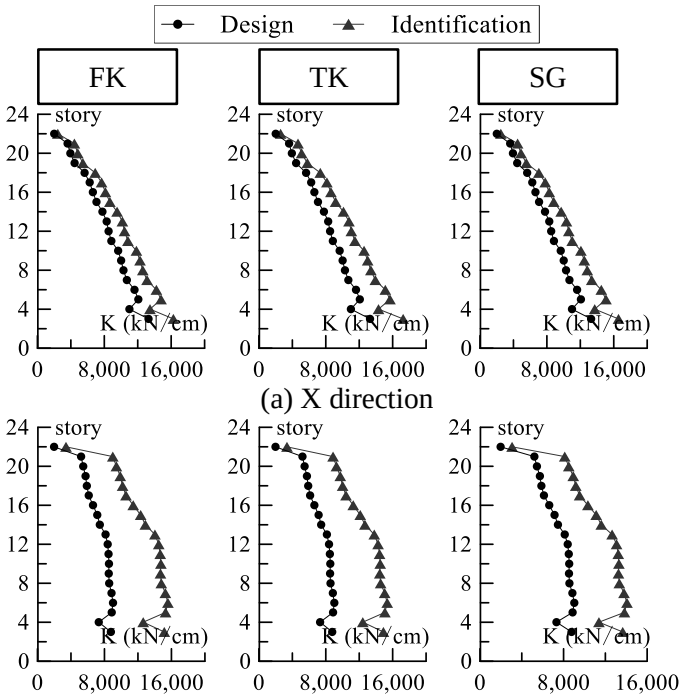

Fig. 12 Story stiffness

4. Identification of seismic isolation layer based on seismic response observation records

4.1 Identification of layer stiffness of base isolated layer

In this section, the stiffness K_0 of the base-isolated layer is calculated by the same method as in section 3.2, but here, the interlaminar deformation δ_0 of the base-isolated layer is directly measured data. The shear force of the base isolation layer is defined as Q_0. Fig. 13 (a) and 13 (b) compare the stiffness K_0 of the base isolation layer in the X and Y directions with the design value. Table 5 shows the value of the magnification β_{K0} given to the design rigidity when identifying the seismic isolation layer in the three observation records. Fig. 14 shows the relationship between β_{K0} and the maximum deformation δ_{0max} of the seismic isolation layer. As shown in Fig. 14, there are variations in both X and Y directions, and the identification values have a width of 1.26 to 1.46 times in the X axis direction and 1.21 to 1.36 times in the Y axis direction.

4.2 Identification of equivalent damping constants using seismic response observation records

As shown in Fig. 15, the equivalent damping constant is calculated from a maximum of one loop of the hysteresis curve. In the hysteresis curve, the equivalent damping constant h_{eq} can be calculated using Eq.(4) [3].

$$h_{eq} = \frac{1}{4\pi}\left(\frac{\Delta W}{W}\right) \tag{4}$$

Here, ΔW is the area of one cycle of the hysteresis loop, and We is the equivalent potential energy, which is calculated as in Eq. (5) using the maximum interlayer displacement δ_{max} and the shear force Q_{0max} at that time.

$$W_e = \frac{1}{2}\cdot\delta_{0\max}\cdot Q_{0\max} \tag{5}$$

If there is a deviation between δ_{0max} and δ_{0min}, adjustment is made so that $|\delta_{max}| = |\delta_{min}|$. Fig. 16 shows the calculated h_{eq}. h_{eq} could not be calculated from the X direction of the Tokaidonanhou-Oki Earthquake (FK). From Fig. 16, it was confirmed that the h_{eq} value was reduced as the maximum amplitude was increased.

The response of the steel damper is below the yield deformation (3.17 cm) and the slip of the oil damper [2]. However, as shown in Fig. 13, the hysteresis curve of the damper has a bulge, and some energy absorption does not occur. You can see that there is. Although this has not yet been identified, it is considered that this is due to the effects of piping and expansion joints. In order to take this effect into account, an analytical model with a viscous element added to the seismic isolation layer and an analytical model with a friction element added are created, compared with observation records, and analyzed for equivalent damping constant of the seismic isolation layer.

Table 5 Magnification for design stiffness (seismic isolation layer)

	FK		TK		SG	
	X	Y	X	Y	X	Y
β_{K0}	1.46	1.21	1.44	1.36	1.26	1.25

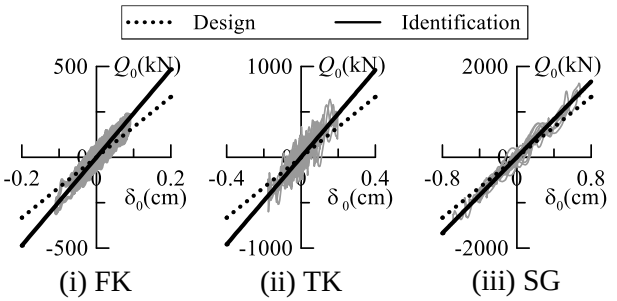

(i) FK (ii) TK (iii) SG

Fig. 13 Histeresis loop of seismic isolation layer (X direction)

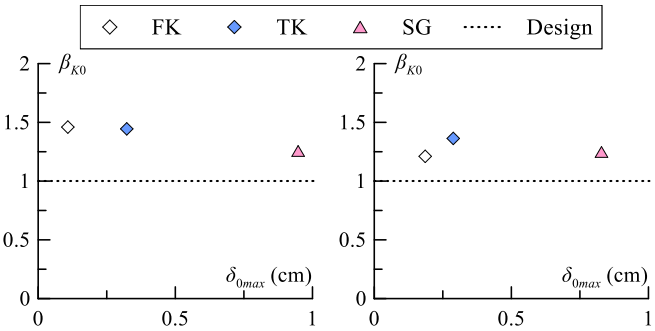

(a) X direction (b) Y direction

Fig. 14 Relationship between β_{K0} and maximum deformation

4.3 Forced displacement analysis method

This section focuses on the total absorbed energy during an earthquake, and describes a method for identifying viscous and frictional elements, respectively. The time history of the absorbed energy of the observed value at the time of the earthquake is calculated by calculating the area of the history loop every moment from the time history of δ_0 and Q_0 referred to in section 4.1. The absorbed energy of the seismic isolation layer of the structural model to be created is calculated using δ_0 as well as the observed values. However, since the vibration equation is based on the balance of forces, it is possible to obtain a response by inputting acceleration and load, but it is not possible to obtain a response by inputting displacement. Therefore, it is necessary to use a

sufficiently high rigidity K_{cont} (K_{cont} = 1.0 x 106 kN / cm) as a displacement control spring and apply dynamic external force to the seismic isolation layer stiffness ($K_f + K_d$) to analyze at the specified displacement. Is used. Fig. 17 shows the restoring force characteristics of the seismic isolation layer. Fig. 18 (a) and 18 (b) show an analytical model for forced vibration in which K_{cont} is expressed in parallel with a model obtained by adding a viscous and frictional element K_R to the seismic isolation layer stiffness ($K_f + K_d$), respectively. As shown in Fig. 18 (a), when a viscous element is added, the load F_{cont} (t) for giving an arbitrary displacement δ_0 (t) is given by Eq. (6).

$$F_{cont}(t) = K_{cont}\delta_0(t) + (K_f + K_d)\delta_0(t) + C_0\dot{\delta}_0(t) \tag{6}$$

Here, since the relationship is as shown in Eq. (7), Eq. (6) can be expressed as Eq. (8) below.

$$K_{cont}\delta_0(t) \gg (K_f + K_d)\delta_0(t) + C_0\dot{\delta}_0(t) \tag{7}$$

$$F_{cont}(t) = K_{cont}\delta_0(t) \tag{8}$$

Next, as shown in Fig. 18 (b), when a friction element is added, the load F_{cont} (t) Eq. (9) for giving an arbitrary displacement δ_0 (t) is obtained.

$$F_{cont}(t) = K_{cont}\delta_0(t) + (K_f + K_d)\delta_0(t) + Q_{Fy}\dot{\delta}_0(t) \tag{9}$$

Here, since the relationship is as shown in Eq. (10), Eq. (9) can be similarly expressed as Eq. (8).

$$K_{cont}\delta_0(t) \gg (K_f + K_d)\delta_0(t) + Q_{Fy}\dot{\delta}_0(t) \tag{10}$$

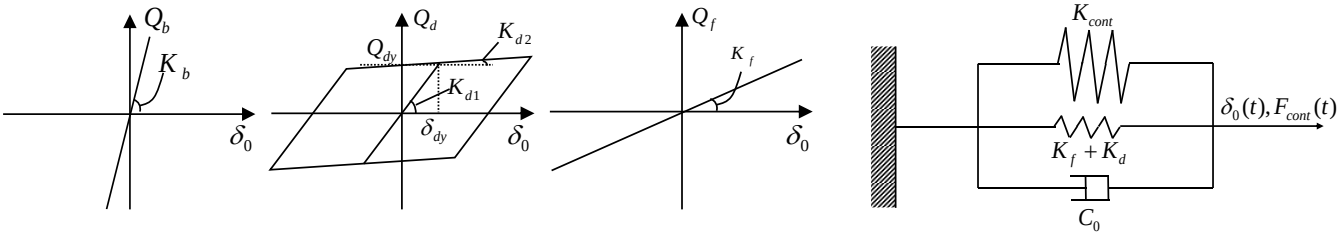

(a) High stiffness (b) Steel damper (c) Natural rubber bearing

Fig. 17 Restoring force characteristics of the base isolation layer

(a) Viscous model

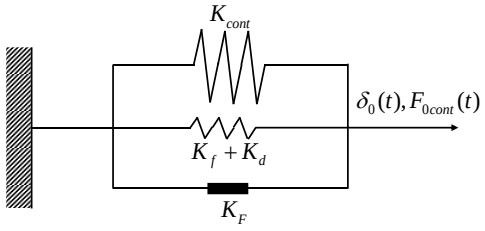

(b) Friction model

Fig. 18 Analytical model

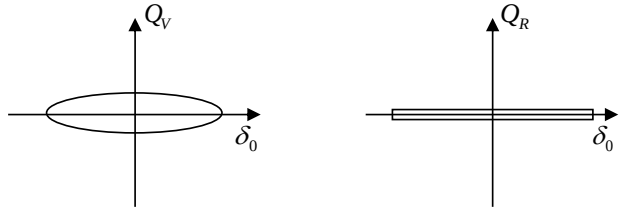

(d) Viscous element (C_0) (e) Friction element (Q_{Fy})

4.4 Identification of damping constant of base isolation layer when viscous element is installed

In this section, the viscous damping coefficient C_0 is identified from the forced vibration analysis. C_0 was determined by trial and error so that the absorbed energy W_0 of the base-isolated layer obtained from the forced displacement analysis was less than 1% of the absorbed energy at the end of the vibration obtained from the observation records.

$$h_0 = C_0 \Big/ 2\sqrt{(K_f + K_d)\cdot M} \tag{11}$$

Here, M is the total mass of the building. Also, for comparison with the equivalent damping constant calculated in section 4.2, calculate the equivalent damping constant h_{eq} of the viscous element from Eq. (5) from the hysteresis curve of the analysis value. Fig. 19 shows the energy time history waveforms of the observed values and the analysis results. From Fig. 19, it can be seen that the end of the energy time history of the Tokaidonanhou-Oki earthquake (TK) and the Surugawan-Oki earthquake (SG) matched, but the rising part did not. Fig. 20 shows the relationship between the equivalent damping constant h_{eq} and the maximum deformation δ_{0max} of the seismic isolation layer. From Fig. 20, it was confirmed that h_{eq} decreases as the amplitude increases. Also, it can be confirmed that there is variation at the same level.

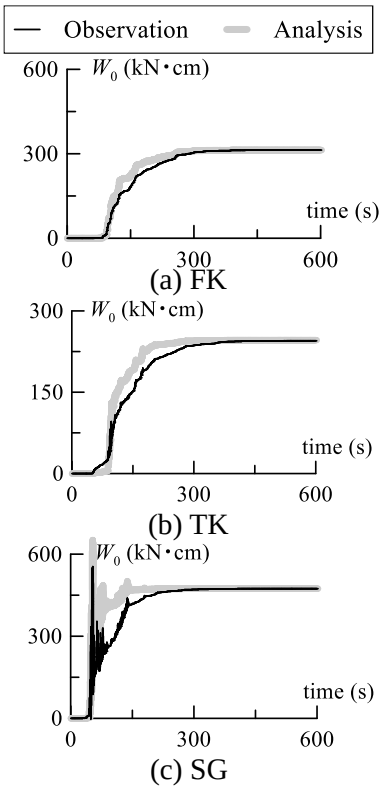

Fig. 19 Comparison of observed energy and absorbed energy of analysis result (X direction)

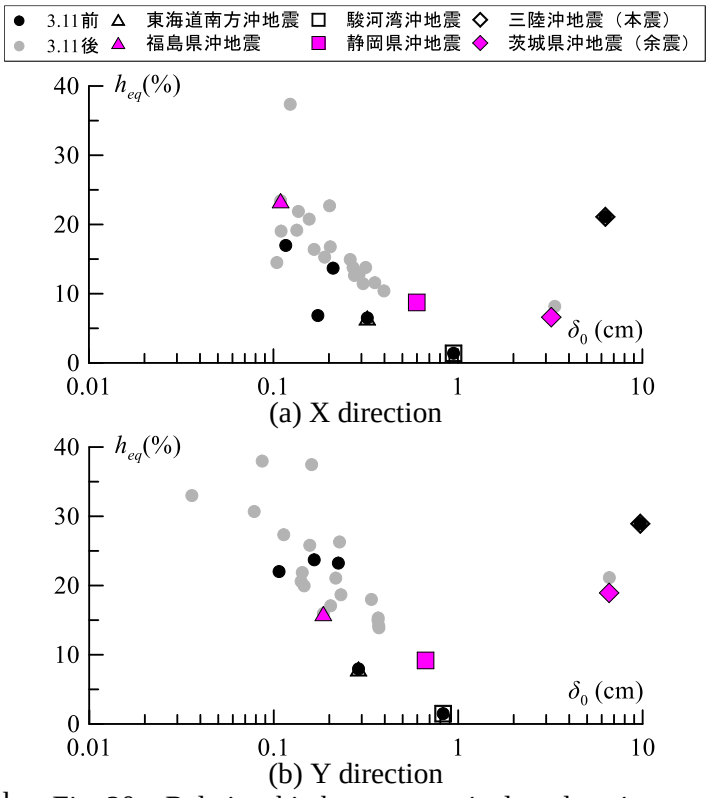

Fig. 20 Relationship between equivalent damping ratio and maximum deformation (Viscous element)

4.5 Identification of damping constant of seismic isolation layer when friction element is installed

In this section, assuming a friction element in the seismic isolation layer as shown in Fig. 18 (a), the shear force coefficient α_{Fy} is identified. The slip load α_{Fy} of the friction element is calculated using Q_{Fy} as in Eq. (12).

$$\alpha_{Fy} = Q_{Fy} / (M \cdot g) \tag{12}$$

Here, g is the gravitational acceleration. The initial stiffness KF of the friction element is calculated as in Eq. (13) using Q_{Fy} and the slip displacement δ_{Fy} of the friction element. In this paper, δ_{Fy} is set to 0.001 cm.

$$F_F = Q_{Fy} / \delta_{Fy} \tag{13}$$

The shear force coefficient α_{Fy} is calculated so that the absorbed energy W_0 of the base-isolated layer obtained from the forced displacement analysis is less than 1% of the absorbed energy at the end of vibration obtained from the observation records. Also, for comparison with the equivalent damping constant calculated in section 4.2, calculate the equivalent damping constant h_{eq} of the viscous element from Eq. (5) from the hysteresis curve of the analysis value. Fig. 21 shows the energy time history waveforms of the observed values and the analysis results. Fig. 21 confirms that not only the end of the energy time history but also the rising part of the Tokaidonanhou-Oki Earthquake (TK) and the Surugawan-Oki earthquake (SG) generally match. Seems reasonable.

Next, h_{eq} is calculated using Eq. (5) as in section 4.2. Fig. 22 shows the relationship between h_{eq} and the maximum deformation δ_{0max} of the seismic isolation layer. From Fig. 22, it was confirmed that the h_{eq} decreases as the amplitude increases, indicating that the amplitude is dependent. Also, it can be confirmed that there is variation at the same level. From the above, it was identified that the h_{eq} when assuming the viscous element was larger than the h_{eq} calculated from the observed displacement values, and the h_{eq} when assuming the friction element was smaller, but the actual seismic isolation layer was not identified by piping or expansion joints. Since it is presumed that the secondary member exists and the viscous element and the friction element are mixed, it is considered reasonable that the h_{eq} calculated from the observed values is an intermediate value between the two.

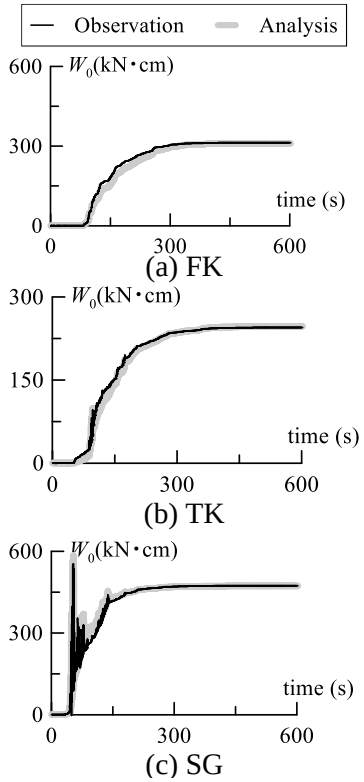

Fig. 21 Comparison of observed energy and absorbed energy of analysis result (X direction)

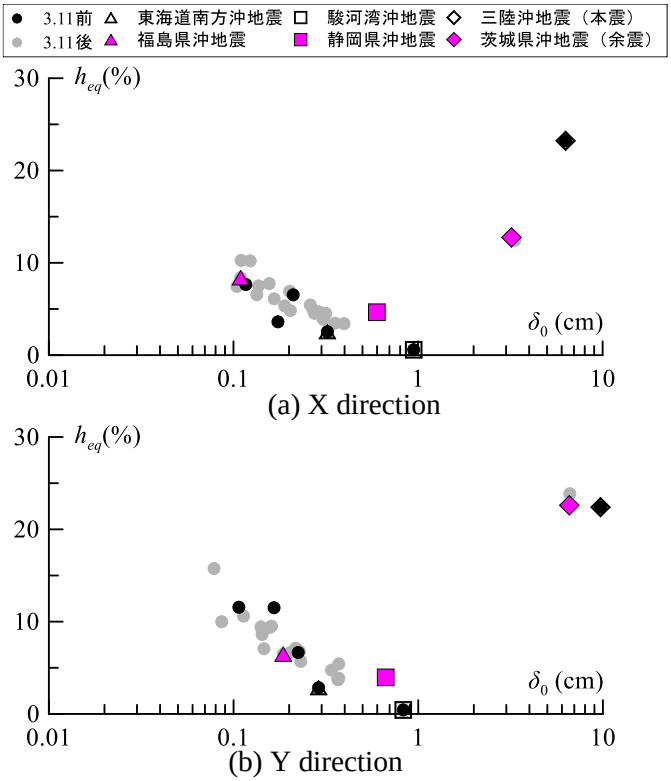

Fig. 22 Relationship between equivalent damping ratio and maximum deformation (Friction element)

5. Earthquake response analysis

5.1 Overview of analysis model

In Chapters 5 and 6, time history response analysis is performed using seven structural models. The structural model is a 22 mass equivalent shear type model shown in Fig.23. One of the structural models is a model based on a design document (hereinafter, a design model). The other six are the models identified in Chapters 3 and 4 (hereafter, identification models). The identification model is a model in which the viscous damping coefficient C_0, which is a viscous element, is added to the seismic isolation layer (hereinafter referred to as the viscous model (Fig. 24 (a))), and a model in which the slip load Q_{Fy} is added to the seismic isolation layer. (Hereinafter, a friction model (Fig. 24 (b))) is used. Here, Ref. 4) correspond to the friction model of FK in this paper. The damping of the design model is assumed to be proportional to the rigidity of the seismic isolation layer 0% and the superstructure 1%. In the viscous model and the friction model, the damping of the seismic isolation layer is C_0 and α_{Fy} identified in Chapter 4, respectively, and the damping of the superstructure is the Rayleigh damping identified in Chapter 3. The time step of the time history response analysis is 0.01 s.

5.2 Response comparison of earthquake observation records and analysis results

In this section, the accuracy of the identification model is evaluated by comparing the analysis results of the identification model of the J2 building with the earthquake observations using the observation records. Fig. 25 shows an example of observation records of the Fukushima-Oki earthquake (FK, Y direction), the acceleration time history waveforms in the Design model, the Friction model, and the viscous model (Viscous model). Fig. 26 shows the distribution of the maximum acceleration $Acc._{max}$ in the height direction. From Fig. 25 and Fig. 26, it can be confirmed that the response of the analysis value of the identification model and the response of the observed value agree well. This indicates that the response in the identification model can accurately reproduce the seismic observation record.

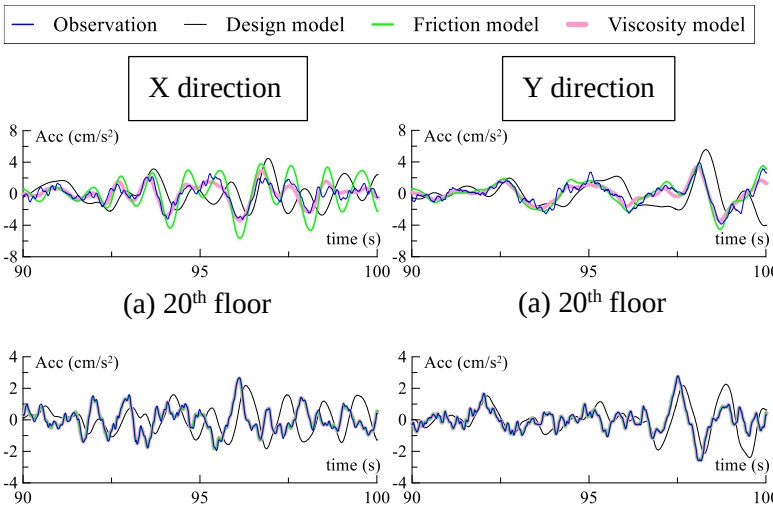

Fig. 25 Time history of acceleration

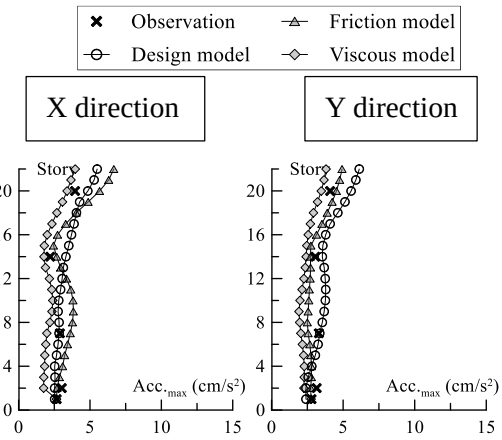

Fig. 26 Maximum acceleration (FK)

6. Conclusion

In this paper, the dynamic characteristics of a building were identified based on multiple seismic response observation records, and the results of the analysis, the design model, and the analysis results of the identification model were compared. In addition, we evaluated each element by comparing it with the observation value of the element added to the seismic isolation layer. The identification model and its analysis results due to the variation in the amplitude of the seismic response observation records were examined, and further improvement in accuracy was confirmed.

7. References

[1] Sato D, Fukuda Y, Kitamura H (2012): Vertical Response Analysis Based on the Observation Earthquake Records for Isolated Buildings. *Journal of Structural and Construction Engineering (Transactions of AIJ)*, **Vol.77**, No.682, 1853-1862 (In Japanese).

[2] Matsuda K, Kasai K (2014): Study on Dynamic Behavior of High-Rise Buildings Based on Its Response Records during the 2011 Tohoku-Oki Earthquake. *Journal of Structural and Construction Engineering (Transactions of AIJ)*, **Vol.79**, No.704, 1445-1455 (In Japanese).

[3] Wu J, Sato D, Fugo Y, Tamura T (2019): Wind Response analysis of A High-Rise Seismically Isolated Building Using Identification Models from Multiple Earthquake Response Observation Records. *Journal of Structural Engineering*, **Vol.65B**, 55-66 (In Japanese).

